Received 25 October 2023; revised 14 December 2023; accepted 25 December 2023. Date of publication 3 January 2024; date of current version 26 March 2024.

Digital Object Identifier 10.1109/OJAP.2024.3349455

An Integrated DRA-Based Large Frequency Ratio Antenna System Consisting of a MM-Wave Array and a MIMO Antenna for 5G Applications

AWAB MUHAMMAD [1], MUHAMMAD U. KHAN [1] (Member, IEEE), REZA SHAMSAEE MALFAJANI [2] (Graduate Student Member, IEEE), MOHAMMAD S. SHARAWI [2,3] (Fellow, IEEE), AND MOATH ALATHBAH [4]

[1]SEECS, National University of Sciences and Technology, Islamabad 44000, Pakistan

[2]Department of Electrical Engineering, Polytechnique Montreal, Montreal, QC H3T 1J4, Canada

[3]Blue Origin, LLC., Kent, WA 98032, USA

[4]Department of Electrical Engineering, College of Engineering, King Saud University, Riyadh 11421, Saudi Arabia

CORRESPONDING AUTHOR: M. U. KHAN (e-mail: umar.khan@seecs.edu.pk)

This work was supported by the Researchers Supporting Project, King Saud University, Riyadh, Saudi Arabia, under Grant RSPD2023R868.

ABSTRACT This paper presents a large frequency ratio antenna that covers the widely separated 5G bands. The proposed antenna consists of a 2-element rectangular DRA (rDRA)-based MIMO antenna for the sub-6 GHz band, with an embedded 1×4 cylindrical DRA (cDRA) array covering the mmW band. The rDRAs are fabricated through a cost and time-efficient 3D printing process, whereas small dimensions of cDRAs are precisely machined through a CNC. The proposed antenna has a measured impedance bandwidth of 31.63% at 4.9 GHz and 21.5% at 28 GHz. The antenna has a peak gain of 6.6 dBi at the sub-6 GHz and 12 dBi at the mmW bands. Moreover, the proposed antenna has an Envelope Correlation Coefficient (ECC) of less than 0.01, whereas the simulated beam steering performance of the antenna exhibits good performance for the sector of ±50°.

INDEX TERMS Large frequency ratio antenna, dielectric resonator antenna, multiple input and multiple output, beamforming, array antenna, 5G.

I. INTRODUCTION

FIFTH Generation (5G) of cellular communication systems is currently being deployed around the world. It is a substantially improved communication standard compared to its predecessors, and primarily offers its users improved bandwidth, ultra-high reliability, low latency, and massive connectivity. These interesting characteristics of 5G standards are crucial in realizing revolutionary technologies such as Vehicle to Everything (V2X), Internet of Things (IoT), smart homes, smart cities, and more. In addition to the commonly used sub-6 GHz band, the 5G standard also aims to benefit from the vacant millimeter-wave band. Therefore, design guidelines of 5G enabling technologies differ for sub-6 GHz and the millimeter-wave band. For instance, Multiple Input and Multiple Output (MIMO) antennas are preferred at the sub-6 GHz band, whereas at the mmW-band, array antennas are a preferable solution. MIMO antennas can offer higher data rates through efficient spectrum resource utilization, which is increasingly becoming scarce at sub-6 GHz. Likewise, array antennas compensate for the additional path loss at millimeter waves by increasing the gain of a single antenna element.

Antenna design is one of the crucial enabling factors for realizing 5G systems. To benefit from both widely separated 5G frequency bands, research in multiband antennas with large frequency ratio antennas is becoming popular. This area is different from conventional approaches of multiband antennas [1], [2], [3], [4], [5], [6], [7], [8], [9], [10], [11], [12], [13], [14], [15], which usually consists of exciting higher order modes in patch antennas and DRAs but have less freedom in controlling the frequency ratio, and radiation patterns at widely separated bands. Hence, to meet the

growing demands and requirements of the wireless industry, new and innovative large-frequency ratio antenna solutions are required to fulfill stringent antenna design criteria.

A straightforward method to achieve a multi-band large frequency ratio antenna is by horizontally placing antennas of different bands side by side to one another [16], [17], [18]. However, this methodology results in antennas having occupied volume equivalent to the sum of independent radiators. A better approach to designing a large frequency ratio antenna involves reducing the overall occupied area or volume by re-using the feed networks or aperture of the lower-band antenna for the upper-band radiator/ feed networks. Such antennas can be further classified into two categories, according to the amount of ports needed for the excitation of each band. Different radiating elements of the complete antenna are excited through a single port in a single-port excitation. In contrast, the separate excitation of each band is called a multi-port design. Compared to separate excitation for separate bands, single excitation-based antennas are uncommon in the literature due to their complexity [19], [20], [21], [22], [23]. Moreover, they require wideband power dividers and additional filters to isolate both bands in a practical system due to the common port for widely separated bands.

Designs with separate ports for separate bands are popular in the literature. Some of the common approaches for designing structure-reuse antennas are stacked [24], [25], [26], embedded [21], [27], [28], dual functional slots [29], [30], [31], [32], and mode-composite structures [19], [33], [34], [35], [36]. The stacked topology consists of different radiators vertically placed upon one another so that they do not interfere with one another. Reference [24] presented a stacked-based antenna that consists of a rectangular patch antenna that also acts as a ground plane for the 8×8 Ku-band array antenna. Reference [25] presented a stacked-based large frequency ratio solution consisting of a K-band (24.2–26.1 GHz) cavity-backed slot array and a dual function frequency selective surface (FSS) that is placed above it at some distance. The FSS is transparent to the K-band radiation and acts as a radiator at the S-band (2.5–2.7 GHz). The embedded approach reduces the overall area occupied by the antenna by inserting the higher band radiators in the lower band antenna. Xin-Hao et al. demonstrated embedded type large frequency ratio antennas by utilizing perforated patches at 3.5 GHz in which mmW arrays of substrate integrated DRA (SIDRAs) [27] and patch antennas [28] were inserted. In the slot-based approaches, the slot is intelligently designed in such a way that it serves different roles at different bands. For instance, in [31], the sub-6 GHz slot antenna behaves as a connected slot antenna array when it is separately excited through a 1×8 power divider. Similarly, [29] utilizes tapered slot structures that serve as radiating element at 28 GHz but serves as a decoupling structure at 2.45 GHz. Mode composite antennas consist of intelligently designed transmission lines or radiating elements that support a particular mode at one frequency and a different mode at another. Usually, they support TEM mode in the lower frequency band and TE_{10} mode in the mmW band. Reference [34] proposed a dual-band leaky-wave antenna consisting of dual-mode composite transmission lines (DMC-TL). The DMC-TL consists of a dual-layered substrate, in which the upper one acts as a thin SIW structure at the mmW band, whereas at the sub-6 GHz frequencies, the SIW portion of the upper substrate and the lower substrate acts as the microstrip transmission line. Similarly, [36] presented the concept of utilizing the outside peripheries of two closely placed SIW-fed mmW slot arrays to excite loop and monopole field distributions at the sub-6 GHz frequencies.

Dielectric Resonators offer unique characteristics of high radiation efficiency, excitation ease, dielectric material-dependent size, and low conductor losses [37]. Furthermore, it is worth mentioning that only a handful of DRA-based large frequency ratio antennas can be found in the literature [38], [39], [40], [41], [42], [43].

A combination of differentially fed slot and substrate integrated DRA has been presented in [38] for ISM band (5.2/ 24 GHz) applications and has a large frequency ratio of 4.6. Similarly, an integrated antenna with a large frequency ratio of 25 was presented in [39]. It introduced the integration of a substrate-integrated cylindrical DRA at 60 GHz and a microstrip patch antenna at 2.4 GHz. The integration of a high-gain mmW Fabry–Perot resonator antenna (FPRA) with a dielectric resonator antenna (DRA) has been investigated in [40] and [41]. In these papers, ISM bands have been targeted, and different methodologies have been presented to integrate DRA operating at 2.4 GHz and FPRA operating at 24 GHz. Recently, a large frequency ratio antenna has also been demonstrated for 5G cell phones in [42]. It consists of wideband dual-polarized DRA arrays at mmW band, a sub-6 GHz antenna made from metal frames, and multi-layered DRA arrays. Lastly, in [43], an integrated antenna consisting of 2×2 bridge DRA in MIMO configuration and sectoral H-plane horn was presented for 3.5 GHz and 28 GHz 5G bands, respectively.

This paper presents a novel, wideband, large frequency ratio SRA, consisting of DRA-based radiators. To efficiently utilize the scarce frequency spectrum of the sub-6 GHz band, the proposed solution consists of 2-element metal-loaded rDRA-based MIMO antennas. In addition, it utilizes a 1×4 cDRA array to minimize the mmW path losses. The proposed antenna is among the very few reported works on large frequency ratio antennas that include MIMO functionality at sub-6 GHz and array functionality at the mmW band [28]. It surpasses these works in impedance bandwidth by utilizing DRA-based radiating elements and has a significantly lower ECC of less than 0.01.

II. ANTENNA GEOMETRY

The complete antenna system is shown in Fig. 1. The integrated antenna consists of two different radiating elements covering two largely separated 5G bands (5G n79 and

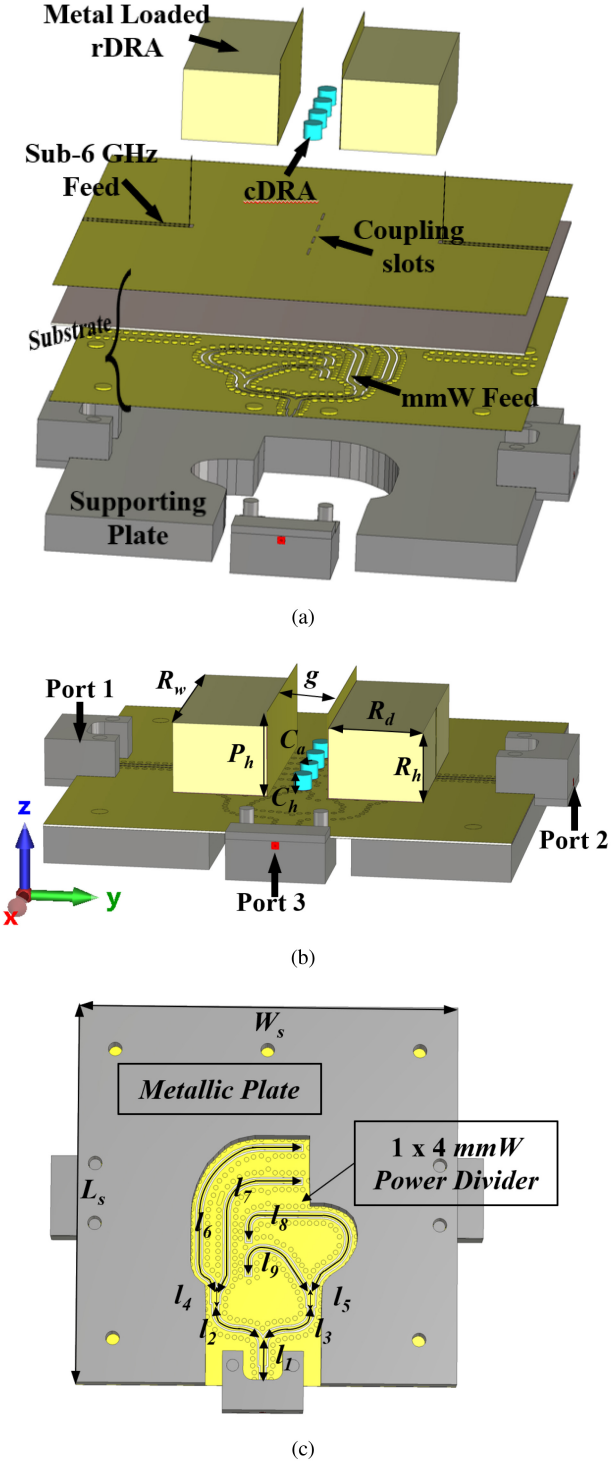

FIGURE 1. Geometry of the proposed large frequency ratio antenna: (a) exploded view, (b) assembled perspective view, and (b) bottom view. (g = 8, R_w = 25, R_d = 12.25, R_h = 9.25, C_h = 2, C_a = 1.2, P_h = 11.3, W_s = 60, L_s = 60, l_1 = 7.37, l_2 = 10.2, l_3 = 10.6, l_4 = 2.1, l_5 = 1.78, l_6 = 32.2, l_7 = 16.4, l_8 = 27.7, l_9 = 35.68. Units are in mm.).

5G n261). At the sub-6 GHz band, the antenna acts as a 2-element MIMO antenna, whereas at the mmW band, a 1×4 array of mmW cDRAs is implemented. The antenna consists of two rDRAs with the relative permittivity of ϵ_{r1} =5, that are glued upon 10 mils Rogers RT/Duroid 5880 substrate and are g =8 mm distance apart from one another. The length, width, and height of the rDRAs are R_w =25 mm, R_d =12.25 mm, and R_h =9.25 mm, respectively. The gap between the rDRAS, is reused to implement a 1×4 mmW cDRA array having relative permittivities of ϵ_{r2} =10. The height, and radius of the cDRAs, are C_h =2 mm, and C_a =1.2 mm, respectively. Thin metal sheets having a length of P_h =11.3 mm are glued with the inside faces of rDRAs to achieve two purposes. Firstly, the plates isolate the rDRAs from getting excited at mmW frequencies, thereby minimizing the radiation pattern distortion at the mmW band. Secondly, the plates also tilt the sub-6 GHz radiation patterns of each rDRA element and reduce their size. The radiating elements are fed through GCPW transmission lines, which are implemented upon a single 60×60×0.254 mm ROGERS® RT/Duroid 5880 substrate. Moreover, the sub-6 GHz feed lines are implemented on the top ground plane of the substrate, whereas the mmW feed network is implemented at the bottom ground plane of the substrate. The sub-6 GHz radiating elements are fed by edge-coupled microstrip probes to excite $TE^x_{\delta 11}$ mode in rDRAs, whereas the mmW cDRAs are fed by a 1×4 T-network through aperture coupling to excite HEM $_{11\delta}$ mode in cDRAs.

III. SUB-6 GHZ ANTENNA DESIGN

The design evolution of the sub-6 GHz antenna is shown in Fig. 2 and is inspired by metal-loaded rDRA presented in [37], [44]. The design starts by designing a simple rDRA for the desired frequency band by utilizing eq. (1) and eq. (2), that are available in [37].

$$F = \frac{f_{GHz}.w_{cm}.\pi.\sqrt{\epsilon_r}}{15} \tag{1}$$

$$F = a_0 + a_1\left(\frac{w}{b}\right) + 0.16\left(\frac{w}{b}\right)^2 \tag{2}$$

where,

$$a_0 = 2.57 - 0.8\left(\frac{d}{b}\right) + 0.42\left(\frac{d}{b}\right)^2 - 0.05\left(\frac{d}{b}\right)^3$$

$$a_1 = 2.71\left(\frac{d}{b}\right)^{-0.282}$$

In eq. (1) and eq. (2), f_{GHz} is the center frequency in GHz, w is the width of rDRA, d is the length of rDRA, b is twice the height of rDRA above the ground plane. By following eq. (1) and eq. (2), a GCPW-fed strip coupled rDRA was designed at the center frequency of 4.7 GHz and is shown in Fig. 2(a), and its E-field is shown in Fig. 2(d). The E-field plot of the antenna shows that it has been excited in the $TE^x_{11\delta}$ mode. The $TE^x_{11\delta}$ mode has symmetrical fields without any nulls and thus results in a broadside pattern.

In the next step, by utilizing image theory, the rDRA was halved, and a metal plate was attached to its other side. The resultant metal-loaded rDRA and its E-field plot are shown in Fig. 2(b) and Fig. 2(e). The field plot shows that the inclusion of a metal plate resulted in a half $TE^x_{11\delta}$ mode

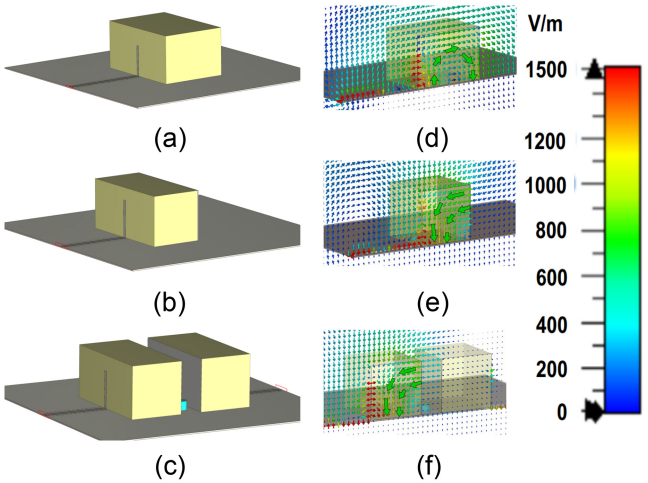

FIGURE 2. Evolution of sub-6 GHz antenna: (a) step 1: rDRA, (b) step 2: metal-loaded rDRA, and (c) step 3: 2-element MIMO metal loaded rDRA. E-field distribution of different cases at $x = 0$ plane: (d) step 1: rDRA, (e) step 2: metal-loaded rDRA, and (f) step 3: 2-element MIMO metal loaded rDRA.

and has a tilted broadside pattern due to the unsymmetrical fields.

Lastly, the metal-loaded rDRA was observed in a 2-element MIMO configuration, and its simulated model and E-field distribution when one of the elements is excited is shown in Fig. 2(c) and Fig. 2(f), respectively. Fig. 2(f) shows that metal-loaded rDRA suits MIMO configuration. The fields in unexcited rDRA are weak and do not contribute to the overall pattern. The space between the plates acts as a cavity and contains strong fields; however, the overall distribution of the field remains unsymmetrical, signifying a tilted pattern.

IV. MILLIMETRE-WAVE ANTENNA DESIGN

This section explores the second half of the antenna design, i.e., the mmW antenna design. It starts from the design equations of a cDRA and extends it to its 1×4 array. Later on, different integration approaches are explored to further characterize the radiation performance at mmW. In addition, this section also explores the beam-steering capability of the antenna and discusses a suitable mmW power divider for the proposed antenna.

A. 1×4 cDRA ARRAY ANTENNA DESIGN AT MILLIMETER WAVES

Firstly, a simple aperture coupled 1×4 cDRA array was made, as shown in Fig. 3. Each cDRA element was excited in $\mathrm{HEM}_{11\delta}$ to have a broadside radiation pattern. The cDRA was designed by utilizing eq. (3) and eq. (4).

$$k_o a(x) = \frac{6.324}{\sqrt{\epsilon_r + 2}}\left(0.27 + 0.36\left(\frac{x}{2}\right) - 0.02\left(\frac{x}{2}\right)^2\right) \quad (3)$$

$$Q(x) = 0.01007\epsilon_r^{1.3}x\left(1 + 100\exp^{-2.05(0.5x - 0.0125x^2)}\right) \quad (4)$$

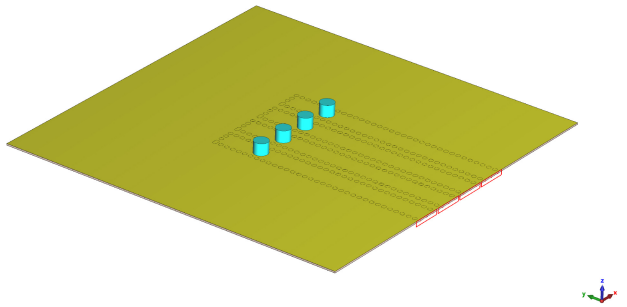

FIGURE 3. Geometry of 1×4 cDRA array.

In eq. (3), $x = a/h$ ranges from 0.125 to 5, whereas in eq. (4), $x = a/h$ ranges from 0.5 to 5.

B. INTEGRATION APPROACHES AND THEIR EFFECT ON MMW PATTERN

The sub-6 GHz and mmW antennas can be integrated together in a number of different ways. Three possible cases and their field plots are shown in Fig. 4. The first case is shown in Fig. 4(a) and consists of an array of mmW cDRAs that are completely embedded in the sub-6 GHz rDRA. This approach has the advantage of tighter integration and only occupies the rDRA area. However, this approach leads to the excitation of higher-order modes in the rDRAs, as shown in Fig. 4(d), signifying a distorted pattern. In addition, the cDRAs are located in a dielectric medium having $\epsilon_r = 5$, due to which their separation decreases from $\lambda_0/2$ to $\lambda_g/2$, accentuating mutual coupling.

In the second case, the rDRA was cut in half and separated to make the surrounding of cDRAs essentially air, as shown in Fig. 4(b). However, as shown in Fig. 4(e), the rDRAs still get excited as they are in the close vicinity of cDRAs. Moreover, the overall fields contain in-phase and out-of-phase regions, signifying distorted radiation patterns at the mmW band.

Metallic plates were used in the third case to isolate the two types of DRAs completely and confine the fields between the rDRAs, as shown in Fig. 4(c). The field plots in Fig. 4(f) verify this approach, in which strong in-phase fields can be observed between the metallic plates. It is worth mentioning that due to fringing from the metallic plates, rDRAs also get excited; however, the relative strength of the fields confined inside the metal plates is much stronger than the field strength of rDRAs. Hence, the utilization of metallic plates substantially improves the field distribution, guaranteeing an undistorted fan-shaped radiation pattern at the mmW band.

C. EFFECT OF PLATE SEPARATION ON MMW PATTERN

The inclusion of plates in combination with the top ground layer converts the separation region into a cavity-like structure [45]. According to [46], the plate separation of an

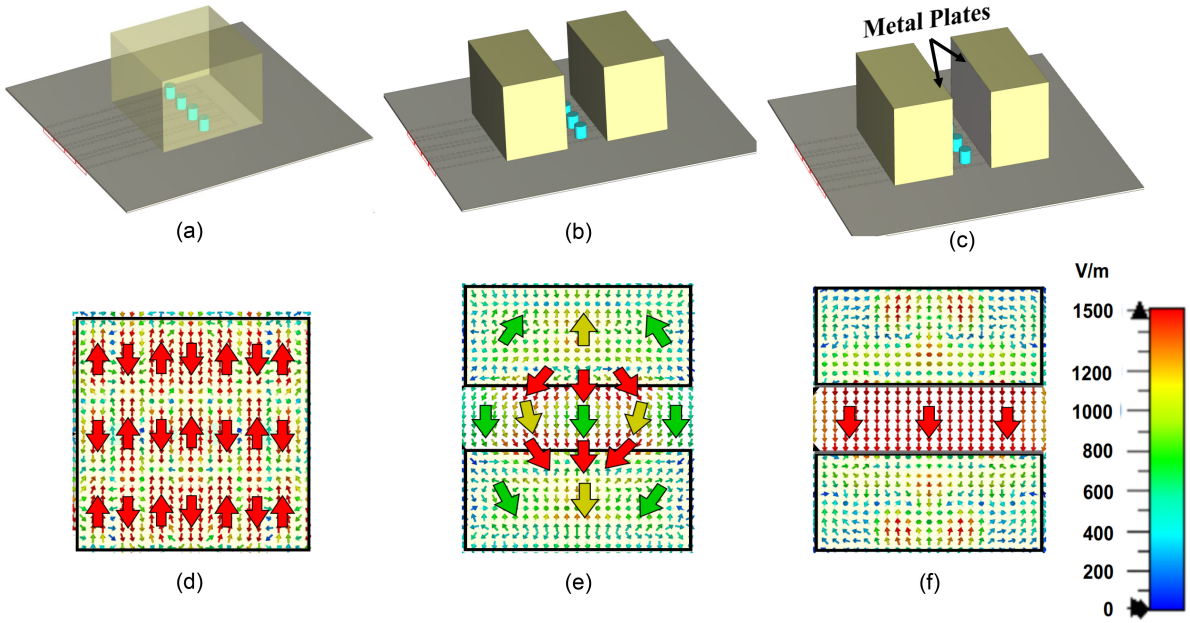

FIGURE 4. Geometries of different approaches to integrate sub-6 GHz and mmW DRAs: (a) Case 1, (b) Case 2, and (c) Case 3. E-field distribution of different cases at $z = h_{DRA}$ plane:: (d) Case 1, (e) Case 2, and (f) Case 3.

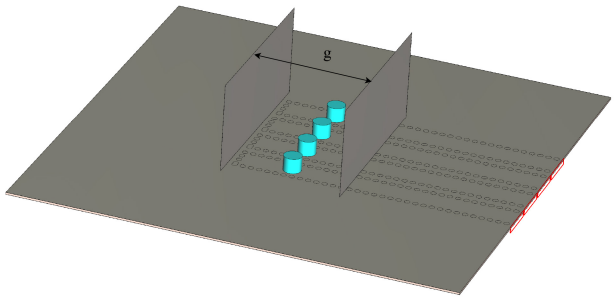

FIGURE 5. Simulation setup for parametric analysis of plate separation effect on radiation pattern.

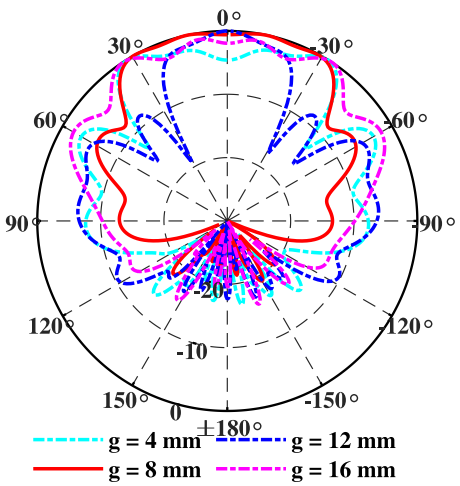

FIGURE 6. Radiation patterns at 28 GHz for different separation of plates.

idealized air-filled cavity having infinite conducting plates that are separated by a distance, g, is given by eq. (5).

$$g = \frac{nc}{2f_0}, \quad for \quad n = 1, 2, 3, \ldots \tag{5}$$

In eq. (5), n is the mode number of the cavity and c is the speed of light in vacuum. At 28 GHz, the plate separation should be 5.4 mm; however, practically, the plates of a cavity are of finite size, and the ideal separation of plates can differ from eq. (5). Therefore, a parametric analysis with various plate separation, g, was studied at 28 GHz, and the simulation model is shown in Fig. 5, whereas the H-plane patterns are presented in Fig. 6. At g = 4 mm, the cavity has a gain of 11.65 dBi, but the peak gain occurs at ±30°. The separation of plates to 8 mm significantly improves the radiation pattern of the antenna and has HPBW = 77.4° with a gain of 11.84 dBi. At g = 12 mm, the HPBW of the pattern reduces to 42.2° and has a gain of 12.7 dBi. Further increase in plate separation, reduces the gain. For instance, at g = 16mm, the cavity has a gain of 10.65 dBi.

D. BEAM-STEERING CAPABILITY

The beam-steering capability of the antenna was also analyzed by exciting each cDRA with different progressive phase shifts tabulated in Table 1. The resultant beams pointing at beam locations ranging from θ_0=0° to ±50° are plotted in Fig. 7, exhibiting a decent coverage of ±50° sector.

E. POWER DIVIDER CONSIDERATIONS

To avoid intersection with sub-6 GHz feed lines, a 1×4 mmW power divider was implemented opposite to

TABLE 1. Phases to steer beam at different location.

Excitation Phases / Beam Locations	Phase 1	Phase 2	Phase 3	Phase 4
$\theta_0 = 0°$	0°	0°	0°	0°
$\theta_0 = \pm 10°$	0°	±31.26°	±62.52°	±93.78°
$\theta_0 = \pm 20°$	0°	±61.56°	±123.12°	±187.68°
$\theta_0 = \pm 30°$	0°	±90°	±180°	±270°
$\theta_0 = \pm 40°$	0°	±115.7°	±231.4°	±347.1°
$\theta_0 = \pm 50°$	0°	±137.89°	±275.66°	±53.66°

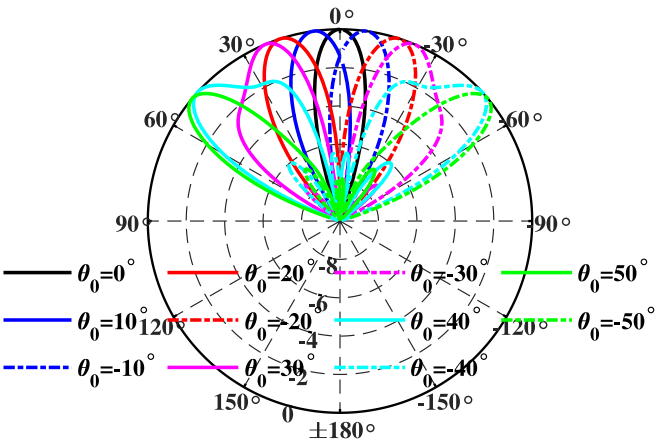

FIGURE 7. Beam steering capability of integrated antenna.

the sub-6 GHz feed lines. Contrary to microstrip/ PCB-based antennas, where the fields are confined in the top and bottom conductors, the DRAs are only glued upon the top ground plane. Therefore, the mmW feed network partially re-uses the area occupied by rDRAs. For better illustration, an overlay view of top and bottom ground planes and top views of DRAs is shown in Fig. 8. The power divider is designed to ensure uniform phase excitation of each cDRA and compensates for two types of phase differences. The first type of phase differences can arise due to the distinct position of each cDRA element from the power divider's starting point. The second type of phase differences can arise due to the oppositely flowing fields in the Set A and Set B branches of the power divider, resulting in a 180° phase difference between them. The optimized dimensions of the power divider are shown in Fig. 1(c).

V. RESULTS AND DISCUSSION

To validate the performance of the proposed antenna, its prototype was fabricated, assembled, and measured at

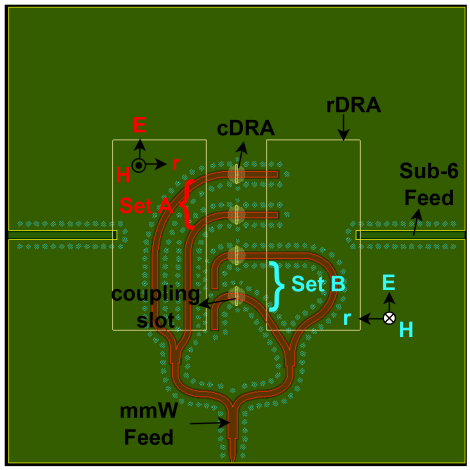

FIGURE 8. mmW power divider considerations.

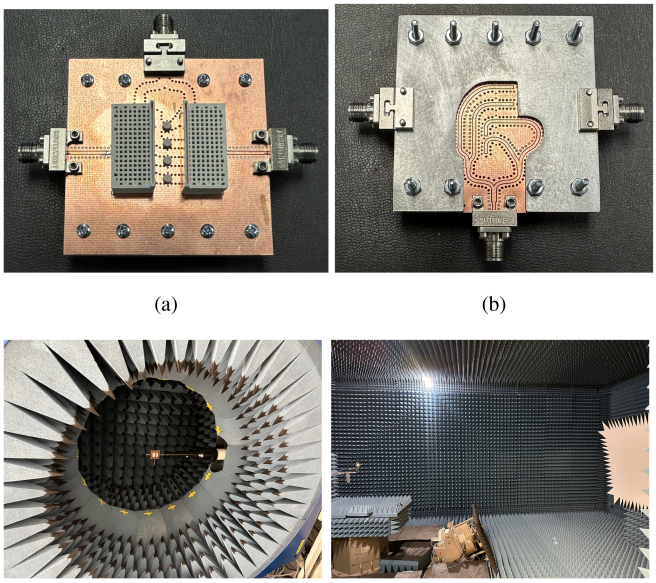

FIGURE 9. Fabricated prototype of antenna: (a) top side, and (b) bottom side. Pattern measurements of the proposed antenna: (c) sub-6 GHz, and (d) mmW.

Polytechnique Montreal, Canada, and is shown in Fig. 9. The rDRAs were 3D printed with a low-loss PREPERM ABS800® filament that has a nominal relative permittivity of 8.0 ± 0.25 and loss tangent of 0.0033. To obtain the desired relative permittivity of 5, 70% nominal infill was used for 3D printing. For cDRAs fabrication, C-Stock AK material from Cuming Microwave having a relative permittivity of 10 and loss tangent of 0.002 was used for CNC machining. S-parameters of the antenna were measured through Keysight THz Vector Network Analyzer (PNA-X to 67 GHz). The sub-6 GHz pattern measurements were done with a near-field Satimo Starlab system, whereas radiation patterns at mmW band were measured in a compact range chamber.

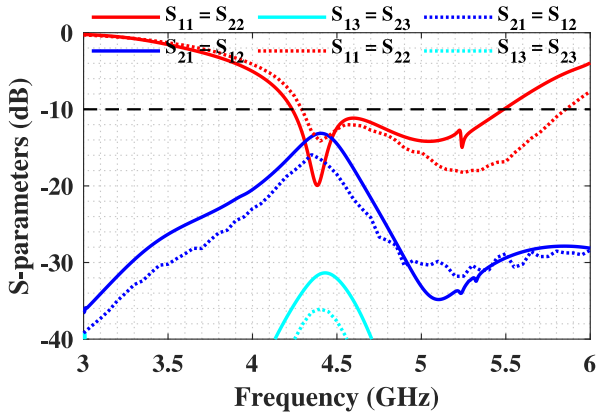

(a)

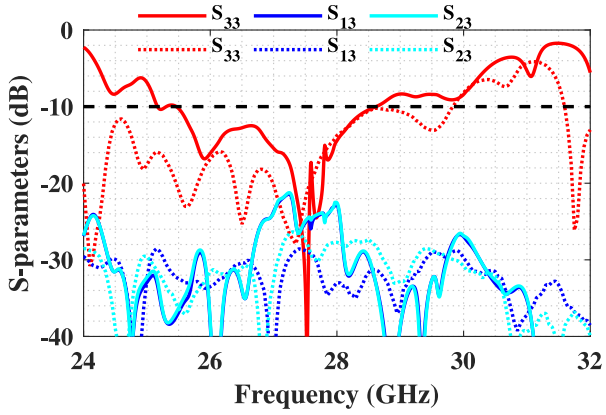

(b)

FIGURE 10. Measured and simulated S-parameters: (a) sub-6 GHz, and (b) mmW band.

A. S-PARAMETERS AND ENVELOPE CORRELATION COEFFICIENT

The S-parameters of the antenna at sub-6 GHz are shown in Fig. 10(a). The antenna has a wide measured −10 dB impedance bandwidth of 31.63% (4.3 GHz-5.85 GHz), whereas the simulated bandwidth is 26.34% (4.3 GHz-5.85 GHz). The antenna has the maximum measured return loss of 19 dB, which is 1 dB less than the simulated one. The simulated port-to-port coupling is less than −12 dB, whereas the measured port-to-port coupling is less than −15 dB. The simulated coupling among the MIMO and mmW feed port is less than −30 dB, whereas the measured coupling is less than −35 dB. Overall, the results prove the suitability of the antenna for the 5G n79 band, which ranges from 4.4 GHz to 5 GHz.

The simulated and measured S-parameters at the mmW band are shown in Fig. 10(b). At these frequencies, the antenna has the simulated −10 dB impedance bandwidth of 12.7% that ranges from 25.1 GHz to 28.5 GHz, whereas the measured impedance bandwidth is 21.5% (24 GHz to 29.8 GHz). The maximum simulated and measured return loss of the antenna is better than −25 dB at 27.5 GHz. These results make the antenna a suitable candidate for the 5G n261 band that ranges from 27.5 GHz to 28.35 GHz. Moreover, isolation among the mmW and sub-6 GHz ports is also shown in Fig. 10(b), which is also less than −20 dB.

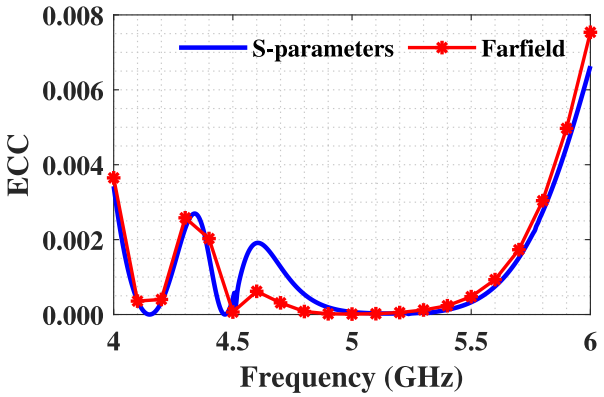

FIGURE 11. Envelope correlation co-efficient (ECC) of the proposed antenna at various sub-6 GHz frequencies.

To further characterize the performance of the antenna, the envelope correlation coefficient (ECC) of the proposed antenna is also obtained through S-parameters and farfields and is shown in Fig. 11. ECC obtained through both approaches is less than 0.01 throughout the sub-6 GHz band and is significantly lower than the value of 0.3, which is set by the standard.

B. RADIATION PATTERNS

The measured and simulated 2D radiation patterns of the MIMO antenna at 4.4 GHz and 5.4 GHz are shown in Fig. 12(a) and Fig. 12(b). At 4.4 GHz, the patterns are tilted to ± 25°, and at 5.4 GHz, patterns are tilted towards ± 61°. This tilt in patterns exhibits spatial decorrelation and is attributed to the metal loading of rDRA elements, as discussed in Section III. The antenna has a peak simulated gain of 7.2 dBi, whereas the peak measured gain is 6.6 dBi.

The E- and H-plane, 2D radiation patterns at 28 GHz and 30 GHz are given in Fig. 12(c) and Fig. 12(d). Due to the limitations in the measurements, measured radiation patterns are only given for the range of ± 90 °. The antenna has a fan-shaped pattern, which is attributed to the rectangular geometry of the cavity. The antenna has the maximum simulated gain of 13 dBi, whereas the peak measured gain is 12 dBi. The antenna has a low sidelobe level of −10 dB and cross-polarization levels of −15 dB. The gain of the antenna at various sub-6 GHz and millimeter-wave frequencies are shown in Fig. 13, exhibiting reasonable performance in simulations and measurements.

C. COMPARISON WITH STATE-OF-THE-ART

A comparison of the proposed antenna's performance with existing works is presented in Table 2. When compared with previous works, the proposed antenna and a recently published [28] are the only papers to utilize MIMO functionality at sub-6 GHz, and an array functionality at the

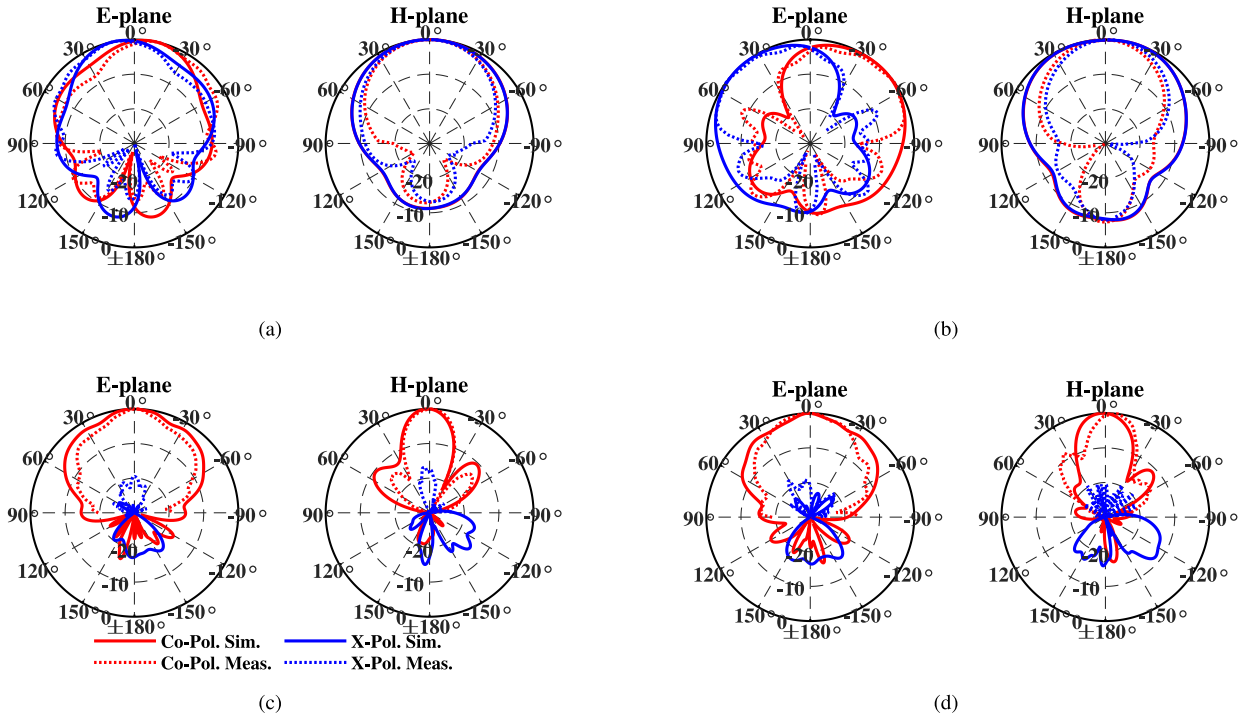

FIGURE 12. Radiation patterns of the proposed antenna at sub-6 GHz band: (a) 4.4 GHz, (b) 5.4 GHz, and (c) 28 GHz, and (d) 30 GHz.

TABLE 2. Comparison of the proposed antenna with the previous works.

Ref.	Antenna Type	Freq. (GHz)	BW (%)	Gain (dBi)	Sub.	Dim. (λ_{01}^3)	Sub-6 GHz MIMO	ECC	MMW Beam Steering
[47]	Magneto-electric (ME) dipole/ FPRA	6.5/ 28	41.6/ 6.66	5.8/ 8.46	3	0.62×0.43×0.14	No	-	No
[48]	Patch/ SIDRAs	3.5/28	11.2/ 13.8	4.8/ 10.8	3	0.45×0.3×0.03	No	-	±50° (Sim.)
[49]	Patch/ ME Dipole	2.4/ 5/ 60	5.7/ 23.4/ 22.6	9.8/ 7.9/ 8.4	3	1.12×1.12×0.1	No	-	No
[28]	Patch/ Patch	3.5/ 28	7.4/ 12.1	6.9/ 14.6	4	0.52×0.94×0.04	Yes	0.03	±25°
[50]	DRA/ DRA	3.6/ 30.5	33/ 27	7.2/ 18	1	0.87×0.87×0.35	No	-	±32°
Proposed	DRA/ DRA	4.9/ 28	31.63/ 21.5	6.6/ 12	1	0.98×0.98×0.18	Yes	<0.01	±50° (Sim.)

Ref. = References; Freq. = Center Frequency; Sub. = Substrate Layers; Sim. = Simulated; BW = Bandwidth; ECC = Envelope Correlation Co-efficient

mmW band. Compared to [28], the proposed antenna offers wider impedance bandwidths due to the utilization of DRA-based radiating elements, comparable gains, better ECC, and a single substrate solution.

VI. CONCLUSION

A large frequency ratio DRA-based antenna consisting of integrated two MIMO rDRA elements and 1×4 cDRA array has been presented in this paper. The antenna covers largely separated 5G n79 (4.4−5 GHz) and n261 (27.5-28.35 GHz) bands. To mitigate the unwanted excitation of rDRAs at the mmW band, metallic plates are used. Moreover, these plates also help in the antenna miniaturization and spatial decorrelation of the MIMO elements at the sub-6 GHz band. The complete antenna is implemented on a single substrate and occupies an area of 60 mm×60 mm, which includes all of the feed networks, rDRAs, and cDRAs. The proposed antenna has reasonable impedance bandwidths of 31.63% and 21.5% and a measured peak

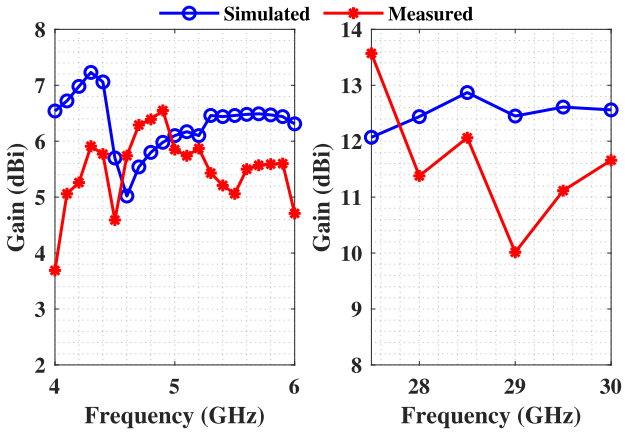

FIGURE 13. Gain of the proposed antenna at various frequencies.

gain of 6.6 dBi and 12 dBi at sub-6 GHz and mmW bands, respectively. Overall, the desirable features of wide impedance bandwidths, moderately high gain, MIMO, and array functionality make the proposed antenna desirable for 5G applications.

ACKNOWLEDGMENT

The authors would also like to acknowledge Polytechnique Montreal support in the fabrication and measurements of the proposed antenna.

REFERENCES

[1] D. Wu, S. W. Cheung, and T. I. Yuk, "A compact and low-profile loop antenna with multiband operation for ultra-thin smartphones," *IEEE Trans. Antennas Propag.*, vol. 63, no. 6, pp. 2745–2750, Jun. 2015.

[2] T. Yue, Z. H. Jiang, and D. H. Werner, "A compact metasurface-enabled dual-band dual-circularly polarized antenna loaded with complementary split ring resonators," *IEEE Trans. Antennas Propag.*, vol. 67, no. 2, pp. 794–803, Feb. 2019.

[3] D. Guha, P. Gupta, and C. Kumar, "Dualband cylindrical dielectric resonator antenna employing $HEM_{11\delta}$ and $HEM_{12\delta}$ modes excited by new composite aperture," *IEEE Trans. Antennas Propag.*, vol. 63, no. 1, pp. 433–438, Jan. 2015.

[4] J. Hao, N. Yan, Y. Luo, H. Fu, and K. Ma, "A low-cost dual-band multimode high-gain stacked-patch antenna based on SISL for 5G applications," *IEEE Antennas Wireless Propag. Lett.*, vol. 21, pp. 4–8, 2022.

[5] B. A. Zeb, N. Nikolic, and K. P. Esselle, "A high-gain dual-band EBG resonator antenna with circular polarization," *IEEE Antennas Wireless Propag. Lett.*, vol. 14, pp. 108–111, 2015.

[6] Y. Liu, X. Li, L. Yang, and Y. Liu, "A dual-polarized dual-band antenna with omni-directional radiation patterns," *IEEE Trans. Antennas Propag.*, vol. 65, no. 8, pp. 4259–4262, Aug. 2017.

[7] B. Feng, L. Li, J.-C. Cheng, and C.-Y.-D. Sim, "A dual-band dual-polarized stacked microstrip antenna with high-isolation and band-notch characteristics for 5G microcell communications," *IEEE Trans. Antennas Propag.*, vol. 67, no. 7, pp. 4506–4516, Jul. 2019.

[8] W. Sun, Y. Li, L. Chang, H. Li, X. Qin, and H. Wang, "Dual-band dual-polarized microstrip antenna array using double-layer gridded patches for 5G millimeter-wave applications," *IEEE Trans. Antennas Propag.*, vol. 69, no. 10, pp. 6489–6499, Oct. 2021.

[9] S. Zarbakhsh, M. Akbari, M. Farahani, A. Ghayekhloo, T. A. Denidni, and A.-R. Sebak, "Optically transparent subarray antenna based on solar panel for cubesat application," *IEEE Trans. Antennas Propag.*, vol. 68, no. 1, pp. 319–328, Jan. 2020.

[10] Q. Wu, J. Yin, C. Yu, H. Wang, and W. Hong, "Low-profile millimeter-wave SIW cavity-backed dual-band circularly polarized antenna," *IEEE Trans. Antennas Propag.*, vol. 65, no. 12, pp. 7310–7315, Dec. 2017.

[11] P. Liu, X.-W. Zhu, Y. Zhang, X. Wang, C. Yang, and Z. H. Jiang, "Patch antenna loaded with paired shorting pins and H-shaped slot for 28/38 GHz dual-band MIMO applications," *IEEE Access*, vol. 8, pp. 23705–23712, 2020.

[12] X.-W. Dai, T. Zhou, and G.-F. Cui, "Dual-band microstrip circular patch antenna with monopolar radiation pattern," *IEEE Antennas Wireless Propag. Lett.*, vol. 15, pp. 1004–1007, 2016.

[13] J.-h. Ou, A. S. Andrenko, Y. Li, Q. Zhang, and H.-Z. Tan, "High-efficiency and wide-frequency-ratio dual-band slot patch antenna utilizing the perturbed TM02 modes," *IEEE Antennas Wireless Propag. Lett.*, vol. 17, pp. 579–582, 2018.

[14] S. Varghese, P. Abdulla, A. M. Baby, and J. P. M., "High-gain dual-band waveguide-fed dielectric resonator antenna," *IEEE Antennas Wireless Propag. Lett.*, vol. 21, pp. 232–236, 2022.

[15] A. A. Khan, M. H. Jamaluddin, S. Aqeel, J. Nasir, J. u. R. Kazim, and O. Owais, "Dual-band MIMO dielectric resonator antenna for WiMAX/WLAN applications," *IET Microw., Antennas Propag.*, vol. 11, no. 1, pp. 113–120, Jan. 2017.

[16] T. Zhihong, Y. P. Zhang, C. Luxey, A. Bisognin, D. Titz, and F. Ferrero, "A ceramic antenna for tri-band radio devices," *IEEE Trans. Antennas Propag.*, vol. 61, no. 11, pp. 5776–5780, Nov. 2013.

[17] L. Zhang, K. Y. See, B. Zhang, and Y. P. Zhang, "Integration of dual-band monopole and microstrip grid array for single-chip tri-band application," *IEEE Trans. Antennas Propag.*, vol. 61, no. 1, pp. 439–443, Jan. 2013.

[18] R. Hussain, A. T. Alreshaid, S. K. Podilchak, and M. S. Sharawi, "Compact 4G MIMO antenna integrated with a 5G array for current and future mobile handsets," *IET Microw. Antennas Propag.*, vol. 11, no. 2, pp. 271–279, 2017.

[19] Y. Su, X. Q. Lin, and Y. Fan, "Dual-band coaperture antenna based on a single-layer mode composite transmission line," *IEEE Trans. Antennas Propag.*, vol. 67, no. 7, pp. 4825–4829, Jul. 2019.

[20] Y. Q. Guo, Y. M. Pan, S. Y. Zheng, and K. Lu, "A singly-fed dual-band microstrip antenna for microwave and millimeter-wave applications in 5G wireless communication," *IEEE Trans. Veh. Technol.*, vol. 70, no. 6, pp. 5419–5430, Jun. 2021.

[21] B. J. Xiang, S. Y. Zheng, H. Wong, Y. M. Pan, K. X. Wang, and M. H. Xia, "A flexible dual-band antenna with large frequency ratio and different radiation properties over the two bands," *IEEE Trans. Antennas Propag.*, vol. 66, no. 2, pp. 657–667, Feb. 2018.

[22] M. Zuo, J. Ren, and Y. Z. Yin, "Dual-band antenna with large frequency ratio based on dual-mode transmission line," *IEEE Antennas Wireless Propag. Lett.*, vol. 20, no. 10, pp. 2068–2072, Oct. 2021.

[23] D. Wang and C. H. Chan, "Multiband antenna for WiFi and WiGig communications," *IEEE Antennas Wireless Propag. Lett.*, vol. 15, pp. 309–312, 2016.

[24] S.-G. Zhou, P.-K. Tan, and T.-H. Chio, "Wideband, low profile P- and Ku band shared aperture antenna with high isolation and low cross-polarisation," *IET Microw. Antennas Propag.*, vol. 7, no. 4, pp. 223–229, Mar. 2013.

[25] J. Zhang, S. Zhang, and G. F. Pedersen, "Dual-band structure reused antenna based on quasi-elliptic bandpass frequency selective surface for 5G application," *IEEE Trans. Antennas Propag.*, vol. 68, no. 11, pp. 7612–7617, Nov. 2020.

[26] T. Li and Z. N. Chen, "Shared-surface dual-band antenna for 5G applications," *IEEE Trans. Antennas Propag.*, vol. 68, no. 2, pp. 1128–1133, Feb. 2020.

[27] X.-H. Ding, W.-W. Yang, W. Qin, and J.-X. Chen, "A broadside shared aperture antenna for (3.5, 26) GHz mobile terminals with steerable beam in millimeter-waveband," *IEEE Trans. Antennas Propag.*, vol. 70, no. 3, pp. 1806–1815, Mar. 2022.

[28] X.-H. Ding, W.-W. Yang, H. Tang, L. Guo, and J.-X. Chen, "A dual-band shared-aperture antenna for microwave and millimeter-wave applications in 5G wireless communication," *IEEE Trans. Antennas Propag.*, vol. 70, no. 12, pp. 12299–12304, Dec. 2022.

[29] M. Ikram, N. Nguyen-Trong, and A. Abbosh, "Multiband MIMO microwave and millimeter antenna system employing dual-function tapered slot structure," *IEEE Trans. Antennas Propag.*, vol. 67, no. 8, pp. 5705–5710, Aug. 2019.

[30] M. Ikram, N. Nguyen-Trong, and A. M. Abbosh, "Realization of a tapered slot array as both decoupling and radiating structure for 4G/5G wireless devices," *IEEE Access*, vol. 7, pp. 159112–159118, 2019.

[31] M. Ikram, E. A. Abbas, N. Nguyen-Trong, K. H. Sayidmarie, and A. Abbosh, "Integrated frequency-reconfigurable slot antenna and connected slot antenna array for 4G and 5G mobile handsets," *IEEE Trans. Antennas Propag.*, vol. 67, no. 12, pp. 7225–7233, Dec. 2019.
[32] E. Al Abbas, M. Ikram, A. T. Mobashsher, and A. Abbosh, "MIMO antenna system for multi-band millimeter-wave 5G and wideband 4G mobile communications," *IEEE Access*, vol. 7, pp. 181916–181923, 2019.
[33] Y. R. Ding and Y. J. Cheng, "A tri-band shared-aperture antenna for (2.4, 5.2) GHz Wi-Fi application with MIMO function and 60 GHz Wi-Gig application with beam-scanning function," *IEEE Trans. Antennas Propag.*, vol. 68, no. 3, pp. 1973–1981, Mar. 2020.
[34] Y. Li and J. Wang, "Dual-band leaky-wave antenna based on dual- mode composite microstrip line for microwave and millimeter-wave applications," *IEEE Trans. Antennas Propag.*, vol. 66, no. 4, pp. 1660–1668, Apr. 2018.
[35] Y. Su, X. Q. Lin, Y. Fan, and K. Wu, "Mode composite sandwich slot line and its applications in antenna development," *IEEE Trans. Antennas Propag.*, vol. 68, no. 6, pp. 4250–4258, Jun. 2020.
[36] Y. Liu, Y. Li, L. Ge, J. Wang, and B. Ai, "A compact hepta-band mode-composite antenna for sub (6, 28, and 38) GHz applications," *IEEE Trans. Antennas Propag.*, vol. 68, no. 4, pp. 2593–2602, Apr. 2020.
[37] A. Petosa, *Dielectric Resonator Antenna Handbook*, Norwood, MA, USA: Artech House, 2007.
[38] Y.-X. Sun and K. W. Leung, "Substrate-integrated two-port dual-frequency antenna," *IEEE Trans. Antennas Propag.*, vol. 64, no. 8, pp. 3692–3697, Aug. 2016.
[39] Y.-X. Sun, K. W. Leung, and J.-F. Mao, "Compact dual-frequency antenna for 2.4/60 GHz applications," in *Proc. Global Symp. Millimeter-Waves*, 2017, pp. 100–102.
[40] L. Y. Feng and K. W. Leung, "Dual-fed hollow dielectric antenna for dual-frequency operation with large frequency ratio," *IEEE Trans. Antennas Propag.*, vol. 65, no. 6, pp. 3308–3313, Jun. 2017.
[41] L. Y. Feng and K. W. Leung, "Wideband dual-frequency antenna with large frequency ratio," *IEEE Trans. Antennas Propag.*, vol. 67, no. 3, pp. 1981–1986, Mar. 2019.
[42] H. Li, Y. Cheng, L. Mei, and L. Guo, "Frame integrated wideband dual-polarized arrays for mm-wave/sub 6-GHz mobile handsets and its user effects," *IEEE Trans. Veh. Technol.*, vol. 69, no. 12, pp. 14330–14340, Dec. 2020.
[43] A. Muhammad, M. U. Khan, Asadullah, and M. S. Sharawi, "A large frequency ratio 2×2 MIMO bridge DRA and millimeter wave H-plane sectoral horn antenna," in *Proc. Int. Conf. Microw., Antennas Circuits (ICMAC)*, 2021, pp. 1–3.
[44] A. A. Kishk and W. Huang, "Size-reduction method for dielectric-resonator antennas," *IEEE Antennas Propag. Mag.*, vol. 53, no. 2, pp. 26–38, Apr. 2011.
[45] K. Lu, Y. Ding, and K. W. Leung, "A new fabry-perot resonator antenna fed by an L-probe," *IEEE Trans. Antennas Propag.*, vol. 60, no. 3, pp. 1237–1244, Mar. 2012.
[46] D. M. Pozar, *Microwave Engineering*, 4th ed., New York, NY, USA: Wiley, 2012, pp. 328–332.
[47] Y.-X. Sun, K. W. Leung, and K. Lu, "Compact dual microwave/millimeter-wave planar shared-aperture antenna for vehicle to-vehicle/5G communications," *IEEE Trans. Veh. Technol.*, vol. 70, no. 5, pp. 5701–5706, May 2021.
[48] W.-W. Yang, X.-H. Ding, T.-W. Chen, L. Guo, W. Qin, and J.-X. Chen, "A shared-aperture antenna for (3.5, 28) GHz terminals with end-fire and broadside steerable beams in millimeter wave band," *IEEE Trans. Antennas Propag.*, vol. 70, no. 10, pp. 9101–9111, Oct. 2022.
[49] X. Yang et al., "An integrated tri-band antenna system with large frequency ratio for WLAN and WiGig applications," *IEEE Trans. Ind. Electron.*, vol. 68, no. 5, pp. 4529–4540, May 2021.
[50] R. S. Malfajani, H. Niknam, S. Bodkhe, D. Therriault, J.-J. Laurin, and M. S. Sharawi, "A 3D-printed encapsulated dual wide-band dielectric resonator antenna with beam switching capability," *IEEE Open J. Antennas Propag.*, vol. 4, pp. 492–505, 2023.

AWAB MUHAMMAD received the B.S. and M.S. degrees in electrical engineering from the National University of Sciences and Technology, Islamabad, Pakistan, in 2018 and 2023, respectively. His research interests include reflectarrays, transmitarrays, multi-beam antennas, DRAs, microstrip patch antennas, large frequency ratio antennas, and higher-order mode antennas.

MUHAMMAD U. KHAN (Member, IEEE) received the M.S. degree in electrical engineering from the GIK Institute of Engineering Sciences and Technology, Topi, Pakistan, in 2008, and the Ph.D. degree in electrical engineering from the King Fahd University of Petroleum and Minerals, Dhahran, Saudi Arabia, in 2015. He is currently an Associate Professor with the School of Electrical Engineering and Computer Science, National University of Sciences and Technology, Islamabad, Pakistan. His research interests include printed antennas and antenna arrays, MIMO antenna systems, and reconfigurable antennas.

REZA SHAMSAEE MALFAJANI (Graduate Student Member, IEEE) received the B.S. degree in electrical engineering from the University of Tehran, Tehran, Iran, in 2009 and the M.S. degree in electrical engineering from Tarbiat Modares University, Tehran, in 2012. He is currently pursuing the Ph.D. degree with the Polytechnique Montréal, Montreal, QC, Canada. He is also a member of the Poly-Grames Research Center, Polytechnique Montréal. His research focuses on the periodic structures, antennas and RF, mm-wave, and terahertz designs. He received the Merit Scholarship Program for Foreign Students (PBEEE) in 2023, the Jocelyne and Jean C. Monty Doctoral Research Excellence Scholarship in 2022, and the Food Agility CRC Scholarship in 2021.

MOHAMMAD S. SHARAWI (Fellow, IEEE) received the M.Sc. and Ph.D. degrees from Oakland University, Michigan, USA, in 2002 and 2006, respectively.

He is currently a Lead Engineer with Blue Origin LLC working on research and development projects for space communication systems. He was a Full Tenured Professor (Professeur titulaire) of Electrical Engineering with Polytechnique Montréal, Montreal, QC, Canada from 2019 to 2023. He was with the King Fahd University of Petroleum and Minerals, Dhahran, Saudi Arabia, from 2009 to 2018, where he founded and directed the Antennas and Microwave Structure Design Laboratory. He was a Visiting Professor with the Intelligent Radio Laboratory, Department of Electrical Engineering, University of Calgary, Calgary, AB, Canada, in Summer–Fall 2014. He was a Visiting Research Professor with Oakland University, Rochester, MI, USA, in 2013 and in 2023. He has more than 400 papers published in refereed journals and international conferences, 11 book chapters (two of which in the Antenna Handbook, fifth edition, McGraw Hill, 2018), one single authored book titled *Printed MIMO Antenna Engineering* (Artech House, 2014), the Lead Author of the book *Design and Applications of Active Integrated Antennas* (Artech House, 2018), and a coauthor of the upcoming book MIMO Antenna Systems for 5G and Beyond (IEEE-Wiley, 2024). He has 28 issued/granted and ten pending patents in the U.S. Patent Office. His research interests include multiband printed multiple-input–multiple-output (MIMO) antenna systems, reconfigurable and active integrated antennas, millimeter-wave antennas, integrated 4G/5G and beyond 5G antenna systems, shared aperture and encapsulated antennas, microwave sensors, applied electromagnetics, sub-THz structures, and computational methods. He was a recipient of the Abdul Hameed Shoman Foundation Award for Arab Researchers for the category of wireless systems in 2020 in addition to various best IEEE conference paper awards. He has served on the Technical and Organizational Program Committees as well as organized several special sessions on MIMO antenna systems and their applications in 4G and 5G wireless systems in several international conferences, such as European Conference on Antennas and Propagation, Antennas and Propagation Society (APS), International Microwave Workshop Series on 5G Hardware and System Technologies, Asia-Pacific Conference on Antennas and Propagation, International Workshop on Antenna Technology, among many others for many years. He has served as the IEEE APS Chair for the Montreal Section from 2020 to 2023 and an Active Member for the IEEE Member Benefits Committee leading the initiative of the APS Student Travel Grant. He is also the Regional Delegate of the EuRAAP in North America. He was an Associate Editor of IEEE ANTENNAS AND WIRELESS PROPAGATION LETTERS from 2019 to 2023. He was the Specialty Chief Editor of the newly launched Frontiers in Communications and Networks for the System and Test-Bed Design Section from 2020 to 2022. He has been serving as an Associate Editor for the IEEE OPEN JOURNAL OF ANTENNAS AND PROPAGATION and *IET Microwaves, Antennas and Propagation* (Wiley), and an Area Editor (antennas and microwave devices and systems) for *Microwave and Optical Technology Letters* (Wiley). He is a Distinguished Lecturer for APS from 2023 to 2025, and a Fellow of IET.

MOATH ALATHBAH received the Ph.D. degree from Cardiff University, U.K. He is currently an Assistant Professor with King Saud University, Saudi Arabia. His research interests include the development of photoelectronic, integrated electronic active and passive discrete devices, the design, fabrication, and characterization of MMIC, RF and THz components, smart antennas, microstrip antennas, microwave filters, meta-materials, 5G antennas, MIMO antennas miniaturized multiband/wideband antennas, and microwave/millimeter components using micro and nano technology.